Excitons in ultrathin organic-inorganic perovskite crystals

Omer Yaffe,[1] Alexey Chernikov,[1] Zachariah M. Norman,[2] Yu Zhong,[2] Ajanthkrishna Velauthapillai,[1] Arend van der Zande,[1] Jonathan S. Owen,[2] and Tony F. Heinz[3,4,*]

[1]*Departments of Physics and Electrical Engineering, Columbia University, New York, New York 10027, USA*
[2]*Department of Chemistry, Columbia University, New York, New York 10027, USA*
[3]*Department of Applied Physics, Stanford University, Stanford, California 94305, USA*
[4]*SLAC National Accelerator Laboratory, 2575 Sand Hill Road, Menlo Park, California 94025, USA*

We demonstrate the formation of large sheets of layered organic-inorganic perovskite (OIPC) crystals, as thin as a single unit cell, prepared by mechanical exfoliation. The resulting two-dimensional OIPC nanosheets of 2.4 nm thickness are direct semiconductors with an optical band gap of 2.4 eV. They exhibit unusually strong light-matter interaction with an optical absorption as high as 25% at the main excitonic resonance, as well as bright photoluminescence. We extract an exciton binding energy of 490 meV from measurement of the series of excited exciton states. The properties of the excitons are shown to be strongly influenced by the changes in the dielectric surroundings. The environmental sensitivity of these ultrathin OIPC sheets is further reflected in the strong suppression of a thermally driven phase transition present in the bulk crystals.

I. INTRODUCTION

Since the introduction of graphene as an excellent platform for fundamental research and applications [1,2], researchers have explored other layered materials that form stable, atomically thin two-dimensional (2D) layers. These 2D materials, such as single- and few-layer insulating hexagonal boron nitride and semiconducting transition metal dichalcogenide crystals, provide electronic and optical properties very different from graphene. Taken together, the individual 2D systems form a library of materials from which vertical and lateral heterostructures can be prepared, opening up intriguing possibilities for the design of materials on an atomic scale with distinctive new properties [3–7].

Here, we explore the optical and excitonic properties of a recent addition to this library: ultrathin crystalline layers of organic-inorganic perovskite crystals (OIPCs). We demonstrate the formation of large (>50 μm^2) layers, with thicknesses down to that of a single unit cell. These materials differ from the previous types of 2D van-der-Waals (vdW) layers in being a hybrid material with an organic compound intrinsically integrated into an inorganic crystal structure. These ultrathin OIPCs thus offer access to the attractive transport and optical properties of 2D inorganic solids, while retaining the flexibility and diversity inherent to organic compounds.

Bulk OIPCs exhibit rich chemical, structural, and optical tunability, arising from the flexibility in combining the inorganic and organic components of the material [8–12]. The basic OIPCs have an AMX$_3$ cubic structure, where A denotes an organic ammonium cation, M a metal cation, and X a halogen anion (Cl$^-$, Br$^-$ or I$^-$) [8]. If the organic cation A is large and cannot fit into the dense cubic crystal, layered A_2MX_4 structures are formed. The layered OIPCs are composed of atomically thin layers of metal halides arranged with strict AB crystallographic stacking and separated by insulating organic ligands, which are coupled through vdW interactions (see Fig. 1) [13–18]. The layered bulk OIPCs have been investigated as naturally occurring direct-gap multiple quantum-well (QW) structures, with the inorganic and organic layers playing the role of the QWs and barriers, respectively [10,19–23]. More recently, optical spectroscopy studies of spin-coated OIPC thin films revealed strong mode coupling in optical microcavities [24,25], demonstrating the potential of OIPCs for photonic applications. However, in order to be effectively incorporated into vdW heterostructures with other 2D materials such as graphene and monolayer transition-metal dichalcogenides, the layers must be isolated in single-crystal form and be both atomically smooth and as thin as possible. In this context, the possibility of producing ultrathin OIPC sheets via mechanical exfoliation was recently reported [26].

Here, we demonstrate the formation of ultrathin crystalline layers of (C$_4$H$_9$NH$_3$)$_2$PbI$_4$ OIPCs by mechanical exfoliation. These exfoliated nanosheets (NSs) are produced by the same mechanical exfoliation technique as has been successfully applied to other van-der-Waals materials, such as transition-metal dichalcogenides and graphene. The NSs are reasonably stable in air (for at least a few minutes) and very stable in vacuum, where they survive repeated temperature cycling. The nanosheets can be produced with lateral dimensions similar to other exfoliated 2D monolayer materials ($\sim$100 μm^2). This enables fundamental studies of the material. For broader application of these materials, new synthetic techniques will be required. Synthesis of large-area OIPC NSs by deposition techniques such as those used for the transition metal dichalcogenides [18,27] may be possible, since bulk OIPCs can be produced via solid-state reactions [8].

The focus of the present study are the optical and excitonic properties of OIPC NSs. The material is shown to be a direct semiconductor, with an optical band gap of 2.4 eV. The band-edge optical transition is excitonic in character and exhibits unusually strong coupling to the optical radiation. At the peak of the main excitonic transition, the NSs with an effective thickness of the inorganic layer of just over a
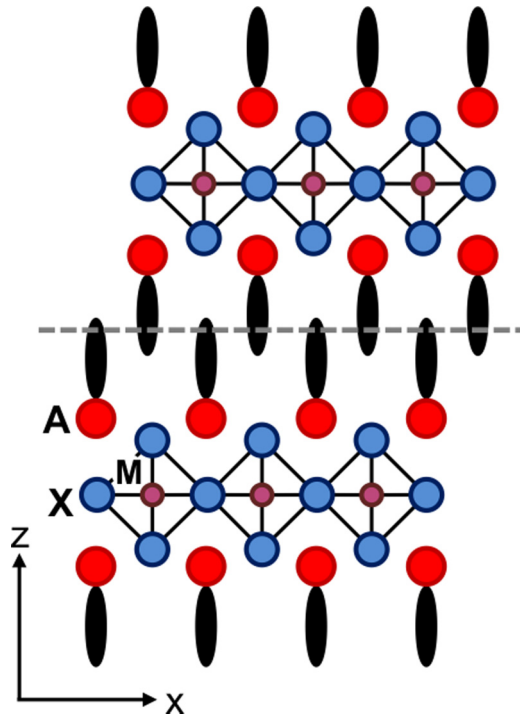
---

*tony.heinz@stanford.edu

FIG. 1. (Color online) Schematic representation of 2D OIPC structure (after Ref. [8]). *A* is an organic ammonium cation, *M* is a divalent metal cation, and *X* is a halogen anion. The dashed line indicates the VdW interface.

nanometer absorb more than 25% of the incident light. By measuring the energies of the excited states of the exciton, we deduce an excitonic binding energy of 490 ± 30 meV for the OIPC-NSs. This binding energy exceeds the value for the corresponding layered bulk material (370 meV) [21,28] and of the cubic three-dimensional OIPC systems (37 meV) [29]. The change in binding energy of both ground and excited excitonic states reflects the influence of the dielectric environment on the screening of charges within the NSs. In addition, we also

observe a suppression of an expected temperature-induced structural phase transition in the OIPC-NSs, highlighting the environmental sensitivity of the material.

II. RESULTS AND DISCUSSION

A. Thin film morphology

Typical layers produced by the exfoliation of bulk $(C_4H_9NH_3)_2PbI_4$ crystals onto SiO_2/Si substrates are found to have lateral dimensions of tens of microns, as shown in the optical micrographs [Fig. 2(a)]. Figure 2(b) presents the image of a typical area of the substrate where several thin layers are present. The contrast profile shows quantized levels, with steplike changes between different areas of the exfoliated flakes. Such behavior reflects the quantized increase in the layer height and is indicative of extremely thin materials, of one to a few layers thickness, as was shown for graphene [30,31] and MoS_2 [32]. Atomic force microscopy (AFM) was used to measure the thickness of the layers with the lowest optical contrast [Fig. 2(c)]. The height profile (inset) reveals a 2.4 (± 0.3) nm step at the edge of a layer. This thickness is compatible with a recent report on exfoliated OIPCs [26] and corresponds well to the 2.8 nm thickness of a single unit cell (i.e., a bilayer) of the bulk material measured by x-ray diffraction (XRD) [33]. The AFM data also show that the roughness of the OIPC layers (root mean square height fluctuations of ~ 0.6 nm) is comparable to that of the underlying SiO_2 (~ 0.3 nm). This demonstrates the material's potential to form intimate interfaces in heterostructures with existing 2D systems such as graphene and the transition-metal dichalcogenides.

B. Absorption and emission spectra

To investigate the electronic and excitonic properties of the $(C_4H_9NH_3)_2PbI_4$ NSs we carried out sensitive optical spectroscopy measurements. The thinnest layers were identified using the correlation between the overall optical contrast
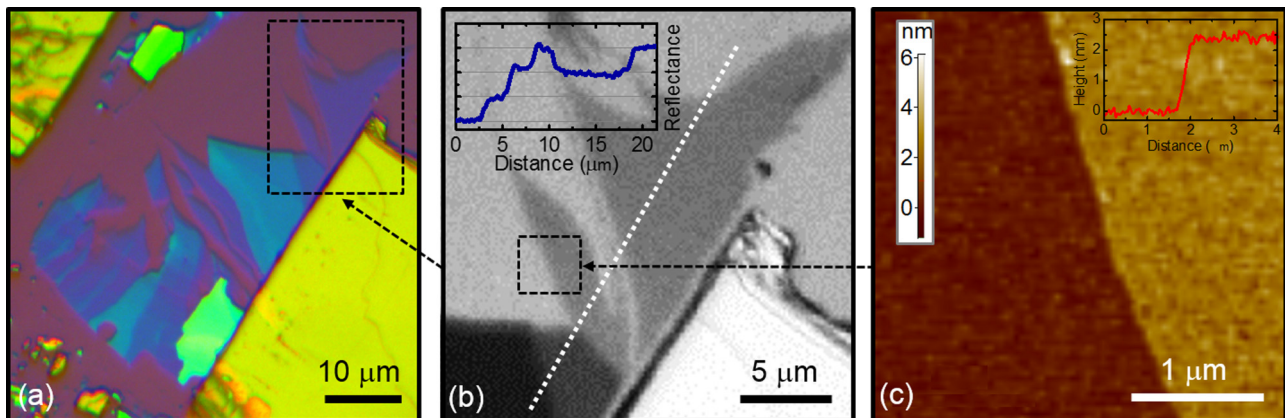

FIG. 2. (Color online) (a) Typical optical micrograph of exfoliated $(C_4H_9NH_3)_2PbI_4$ films deposited on SiO_2(280 nm)/Si substrates. (b) A magnified image of the area indicated by the black rectangle in (a). In this image, only the red channel of the camera is presented and a monochrome presentation is used. The inset of (b) shows the reflectance intensity profile along the white dotted line. Equal steplike changes are observed, as expected for materials of a few monolayers thickness on a SiO_2/Si substrate [30]. (c) AFM topography image for the black rectangle indicated in (b), including the boundary between the two areas with the lowest contrast. The height profile (inset) shows a step of 2.4 nm height at the boundary.
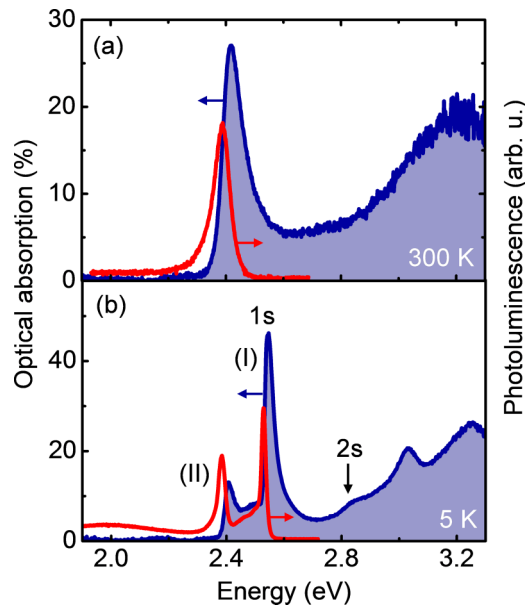
FIG. 3. (Color online) (a) Room-temperature optical absorption and photoluminescence spectra of an exfoliated $(C_4H_9NH_3)_2PbI_4$ NS. (b) Optical absorption and PL from an OIPC-NS at 5 K. The contributions from the two phases are indicated by (I) and (II).

in the micrographs and thickness measured in AFM scans. Figures 3(a) and 3(b) present the optical absorption and photoluminescence (PL) spectra of OIPC-NSs at temperatures of 300 K and 5 K, respectively. Both the absorption and PL spectra are dominated by a strong excitonic resonance at 2.4 eV, consistent with the direct-gap nature of the OIPCs [19,34], with the fundamental transition at the Γ point of the Brillouin zone [10]. The material's absorption at higher photon energies is mainly attributed to a manifold of optical transitions corresponding to higher-lying states across the Brillouin zone [35,36]. Additional resonances, with an energy separation on the order of an eV, may arise from the spin-orbit splitting of the conduction and valence bands at the Γ point [37].

The fluorescence quantum efficiency is estimated from consideration of the excitation and collection efficiencies to be ∼1% (with an error of about one order of magnitude) at room temperature and several percent to 10% at $T = 10$ K. The comparison of the PL and absorption spectra reveals a Stokes shift of 10–20 meV, indicating negligible influence of disorder and inhomogeneity. The additional peak (II) below the main ground-state resonance (I) in the low-temperature spectra is related to the temperature-induced phase transition, as discussed in more detail below. Contributions from the luminescent defect states appear as weak broadband emission below the optical band gap and are strongly quenched at higher temperatures. These observations indicate that the principal PL from the OIPC-NSs is intrinsic in nature and of excitonic origin at all temperatures. Furthermore, the quantum efficiency of the NSs as a function of layer thickness (not shown) appears to be relatively constant. Thus, the quality of the NSs is well preserved in comparison to the bulk, with a relatively low density of defect states.

The most striking feature of the OIPC-NS response is the extremely strong absorption at the excitonic transition, peaking at 25% at room temperature with a spectral broadening of about 0.1 eV. These results were reproduced on more than a dozen samples (see Fig. S4 in the Supplemental Material (SM) [38] for additional details). Taking into account the reduction of the effective electric field at the surface of the dielectric substrate [39], we estimate the intrinsic absorption that one would measure for a suspended layer, to be even higher, at about 37%. This remarkably high absorption is similar and directly related to the exceptionally strong light-matter coupling reported for these materials in the bulk [19,21,24]. Considering the thickness of the absorbing inorganic layers of about 0.65 nm and neglecting multiple reflections, the extracted area of the absorption coefficient, proportional to the oscillator strength, is $2.2(\pm0.3)\times10^5$ eV/cm for the studied supported samples. This is more than two orders of magnitude larger than the corresponding values reported for typical inorganic quantum well (QW) systems, such as GaAs and GaInAs [40,41].

The high absorption strength of the OIPCs can be understood largely in terms of a quantum confinement effect for the subnanometer thickness of the inorganic layers compared to the typical widths of GaA QWs of several nanometers. The strong dependence of the oscillator strength on the QW width is attributed to the increased overlap of the electron and hole wave functions. To illustrate this effect, we extrapolate the GaAs data reported in Ref. [40] down to the thickness of the inorganic OIPC layers. We find an increase in the exciton absorption of more than 1.5 orders of magnitude. Additional contributions are expected to originate from the differences in the dielectric screening, as well as in the carrier effective masses. Furthermore, the exciton oscillator strengths in OIPC NSs are a factor of 2–3 larger than those measured for monolayer metal dichalcogenide crystals (Fig. S5 in the Supplemental Material) [5].

C. Exciton Rydberg series and binding energy

Like the oscillator strength, the exciton binding energy is also strongly influenced by the effect of quantum confinement and the dielectric environment. Quantum confinement restricts the spatial extent of the exciton wave function in the perpendicular direction. It yields a maximum increase of the exciton binding energy by a factor of four in a 2D system compared to the 3D counterpart (without any change in the electron-hole interaction) [42]. An additional contribution to the excitonic binding energy arises from the nonuniform dielectric environment, since the electric field between the electron and hole forming an exciton extends outside the inorganic layer into the surrounding medium [43]. This picture is supported by the Bohr diameter of the 1s exciton in bulk material of 2.8 nm [20], which is comparable to the layer thickness. The resulting screening is typically described by an effective dielectric constant, an average of the dielectric screening of the organic and inorganic layers normalized by their respective thicknesses. In the OIPCs, the smaller dielectric constant of the organic layers leads to decreased screening between the electron and the hole and, thus, to an
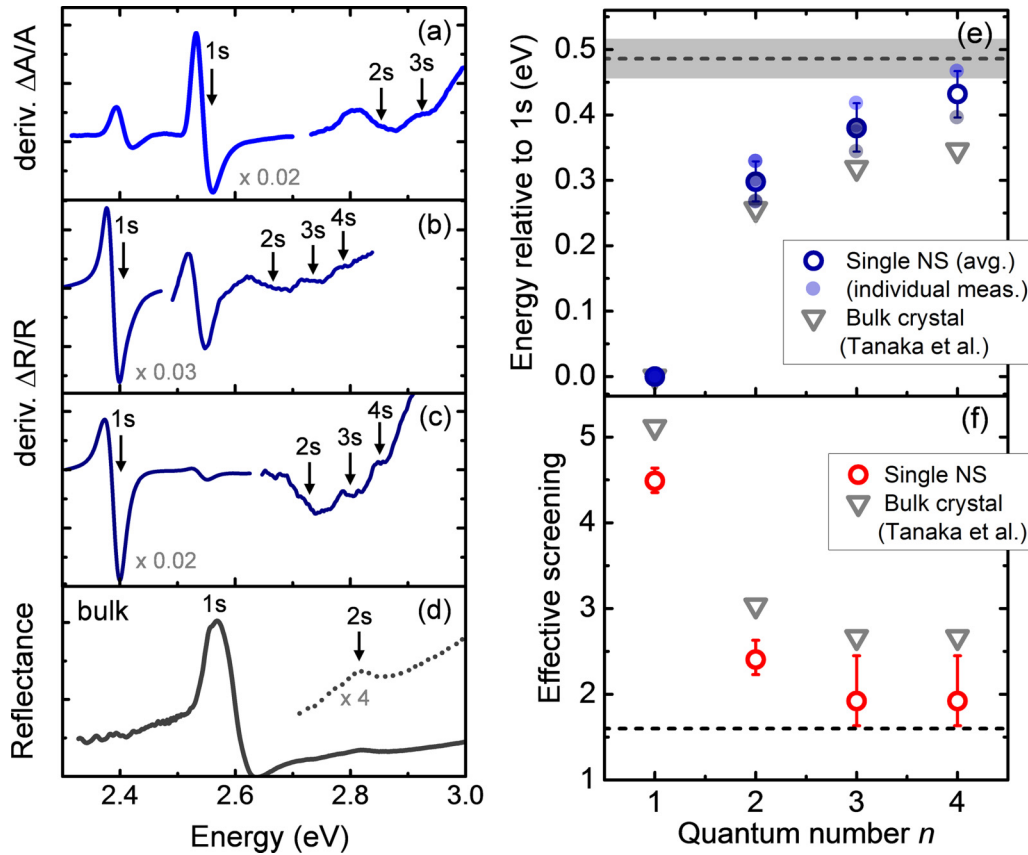
FIG. 4. (Color online) (a) Derivative of the absorption spectrum of the OIPC-NS sample at the temperature of $T = 5$ K (from the data in Fig. 3). The data are rescaled in the spectral range of the ground state resonance for clarity. The optically active exciton states are denoted by $1s$, $2s$, $3s$, and $4s$. (b), (c) Derivatives of the reflectance contrast spectra of two additional OIPC NS samples at $T = 5$ K. (d) Low-temperature reflectance spectrum of a thick bulk sample. The exciton ground state and the first excited state are indicated by $1s$ and $2s$, respectively. (e) Energies of the excited states of the exciton relative to the $1s$ transition for an OIPC-NS compared with the results for the bulk crystals (literature data taken from Ref. [21]). The averaged data (open circles) are presented together with the results from individual measurements on different NS samples (closed circles). The quasiparticle band gap in the OIPC-NS, obtained from the fit of $n = 3,4$ states, is indicated by the dashed line. (f) Effective dielectric screening for the measured exciton states. The error bars originate from the experimental uncertainties in the extracted $3s$ and $4s$ peak positions. The dashed lines indicate the averaged dielectric constant of fused silica substrate ($\epsilon = 2.13$) and vacuum ($\epsilon = 1$) at optical frequencies.

additional increase of the exciton binding energy beyond the prediction for an idealized 2D system [19,23,28,34,44].

To probe the excitonic properties of the NSs, we measured the excitonic Rydberg series, that is, the excited states of the exciton. The allowed single-photon transitions typically involve excitonic states with zero angular momentum, which we label in analogy to the hydrogenic series by the principal quantum number as $2s$, $3s$, etc. [42,45]. The coupling of these excited states to light is significantly reduced compared to the ground-state transition. Hence, high-quality samples and reduced temperatures are typically required for their observation. To that end, the energy derivative of the absorption spectrum of an OIPC-NS at $T = 5$ K is plotted in Fig. 4(a), where the excitonic states are indicated by arrows. Derivatives of the reflectance contrast spectra (reflectance relative to that of the underlying substrate) of two additional samples are presented in Figs. 4(b) and 4(c), illustrating the distribution in the energies of the excited states in different flakes. The reflectance spectrum of a thick bulk crystal is shown in Fig. 4(d) for comparison. The respective energies of the excited

states relative to the $1s$ transition as function of the quantum number n are summarized in Fig. 4(e). The averaged data are plotted together with the results from individual measurements on different NS samples. The data with the largest and smallest peak energies (further indicated by the error bars) correspond to the spectra presented in Figs. 4(b) and 4(c), respectively. For comparison, we also display results for the bulk crystal [21], as reproduced by the measurements of the thick samples [Fig. 4(d)]. Interestingly, the exciton excited states ($2s$, $3s$, and $4s$) in the OIPC-NSs are significantly higher in energy than the corresponding transitions in the bulk.

The exciton binding energy is defined as the energy difference between the ground ($1s$) state of the exciton and the ionization continuum, that is, the quasiparticle band gap for the excitation of free electrons and holes. The position of the continuum is obtained from the extrapolation of the measured series of the excited exciton states. In particular, we determine the energy of the continuum by a fit of the $3s$ and $4s$ excited exciton state to a 2D hydrogenic model, a procedure shown to apply in the previous studies on thick OIPC

crystals [21]:

$$E_n = \text{Ry} \frac{\mu}{\epsilon^2 (n - 0.5)^2}, \qquad (1)$$

where E_n is the energy of the nth state, $\text{Ry} = \frac{m_e e^4}{8 \epsilon_0^2 h^2} = 13.6$ eV is the Rydberg unit of energy, μ is the exciton effective mass in units of the mass m_e of the free electron, and ϵ is the dielectric constant. From this procedure with measured energies of $E_{3s} = 380$ meV and $E_{4s} = 430$ meV relative to the $1s$ transition, we obtain a binding energy for the $1s$ exciton in the OIPC-NS of 490 (± 30) meV. This value is indeed significantly higher than 360 meV reported for similar bulk crystals.

To illustrate the influence of the dielectric environment, we introduce the concept of an effective n-dependent screening. Using an exciton reduced mass of $\mu = 0.18$ [20] and the extracted binding energy of the $1s$ state of 490 meV, we determine the n-dependent dielectric constant ϵ_n required to reproduce the experimental binding energies E_n from the hydrogenic model of Eq. (1). The results are presented in Fig. 4(f), where the effective screening constant of the OIPC-NS is compared to that of the bulk material [21]. In a homogeneous dielectric (as, for example, in conventional GaAs QWs), the effective screening of all excitonic states would be identical. In contrast, both the OIPC-NS and bulk crystals exhibit the same qualitative behavior: The effective screening ϵ_n falls with increasing n, reaching a significantly lower asymptotic value. Since the size of the exciton increases n, this result indicates stronger screening for small electron-hole separations and weaker screening for large separations. This effect is expected for screening within a thin layer (the inorganic component) having a higher dielectric function than that of the surround media [43,46–48]. In particular, the $1s$ exciton, with the smallest size, is affected largely by the screening within the inorganic layer, while the higher excited states are more influenced the external media [21,49].

In bulk OIPCs, the dielectric environment is mainly defined by the presence of the additional organic and inorganic layers. The measured dielectric constant of the bulk material is ~3 [22,29,50]. In NSs, however, the dielectric surroundings are strongly affected by the presence of the substrate on the one side of the layer and vacuum on the other, as reflected in the strong decrease of the asymptotic value, which approaches the average of the dielectric constants of vacuum/air and fused silica [Fig. 4(f), dashed line]. This effect of the dielectric screening is more pronounced for the higher excited states and is the main reason for the overall increase of the binding energy. Recently, similar excitonic effects have also been predicted theoretically [51–56] and observed experimentally [57–60] in atomically thin transition-metal dichalcogenides. The excitonic states in these systems are also strongly influenced by the dielectric environment, leading to binding energies of many hundreds of meV.

D. Phase transition

In addition to the influence of the local environment on the electronic properties of the OIPC-NSs via dielectric screening, the interface between the NS and substrate also modifies the material's structure. A general property shared by many OIPCs
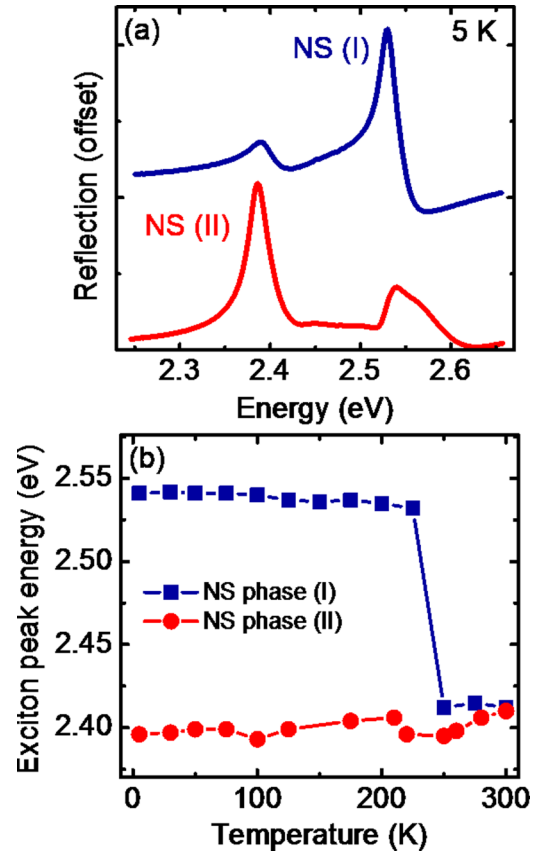

FIG. 5. (Color online) (a) Reflectance spectra for the two types of NSs at $T = 5$ K. (b) The corresponding evolution of exciton peak energies with temperature.

is a structural phase transition, which occurs at temperatures slightly below room temperature. This phase transition is thought to be driven by the ordering of the alkyl-ammonium chains [19] and results in an abrupt shift in the crystal structure and, correspondingly, of the optical gap [8,19]. For the OIPC studied here, the bulk transition temperature is 250 K, where a ~100 meV blue shift of the main exciton resonance is observed [19]. While this phase transition is always present in bulk, it was only observed in about a half of the measured NSs. Typical reflectance spectra of the two representative classes of OIPC-NSs are shown in Fig. 5(a), and the corresponding evolution of the exciton ground state with temperature is presented in Fig. 5(b). In the case of the NSs, we observe two classes of ground-state transitions at cryogenic temperatures: one in which the dominant excitonic resonance appears at 2.53 eV [denoted as (I)] and another in which the dominant transition appears at 2.39 eV [denoted as (II)]. Domains of both phases may coexist within a single flake, which manifest itself as weak features at the resonance energy of the respective opposite phase [Fig. 5(a)]. The temperature dependence clearly shows that the type I materials undergo the phase transition, while the type II materials do not. The frequent observation of the type II flakes suggests that the intimate contact between the NS and the substrate inhibits the phase transition. In addition, aside from the overall spectral shift of the optical resonances, no clear evidence of different exciton binding energies for the two phases is observed within our experimental accuracy.

III. CONCLUSION

In summary, we studied optical and excitonic properties of nanosheets of hybrid organic-inorganic perovskite-type $(C_4H_9NH_3)_2PbI_4$ crystals. These ultrathin layers with the active material thickness on the order of a nanometer are found to exhibit optical absorption up to 25% and bright photoluminescence both at cryogenic and room temperatures. The change in the dielectric environment of these ultrathin films leads to an increase in the exciton binding energy to 490 meV, about 1/3 greater than for the corresponding bulk material. Furthemore, a thermally driven structural phase transition present in the thick OIPC samples is suppressed in the ultrathin layers, indicating a strong interaction of the organic part with the environment. These properties, combined with the additional flexibility associated with the hybrid organic/inorganic nature of the material, make the OIPC-NSs an attractive addition to the family of existing 2D semiconductors. From a fundamental perspective, the strong Coulomb interaction combined with the possibility of electrostatic gating render these materials attractive for investigating novel many-body optical and transport physics in hybrid materials, as well as studying their surface and interface properties. In emerging applications, the OIPC-NSs can be easily incorporated into new vdW heterostructures to provide customizable components for novel devices.

[1] A. K. Geim, Science **324**, 1530 (2009).

[2] A. K. Geim and K. S. Novoselov, Nat. Mater. **6**, 183 (2007).

[3] Q. H. Wang, K. Kalantar-Zadeh, A. Kis, J. N. Coleman, and M. S. Strano, Nat. Nanotech. **7**, 699 (2012).

[4] K. S. Novoselov, V. I. Fal'ko, L. Colombo, P. R. Gellert, M. G. Schwab, and K. Kim, Nature (London) **490**, 192 (2012).

[5] A. K. Geim and I. V. Grigorieva, Nature (London) **499**, 419 (2013).

[6] S. Z. Butler, S. M. Hollen, L. Cao, Y. Cui, J. A. Gupta, H. R. Gutiérrez, T. F. Heinz, S. S. Hong, J. Huang, A. F. Ismach, E. Johnston-Halperin, M. Kuno, V. V. Plashnitsa, R. D. Robinson, R. S. Ruoff, S. Salahuddin, J. Shan, L. Shi, M. G. Spencer, M. Terrones, W. Windl, and J. E. Goldberger, ACS Nano **7**, 2898 (2013).

[7] D. Jariwala, V. K. Sangwan, L. J. Lauhon, T. J. Marks, and M. C. Hersam, ACS Nano **8**, 1102 (2014).

[8] D. B Mitzi, in *Progress in Inorganic Chemistry*, edited by Kenneth D. Karlin (Wiley, New York, 1999), Vol. 38, Chap. 1.

[9] D. B. Mitzi, K. Chondroudis, and C. R. Kagan, IBM J. Res. Dev. **45**, 29 (2001).

[10] G. C. Papavassiliou, Mol. Cryst. Liq. Cryst. Sci. Technol, Sec.A. M **286**, 231 (1996).

[11] C. C. Stoumpos, C. D. Malliakas, and M. G. Kanatzidis, Inorg. Chem. **52**, 9019 (2013).

[12] S. Zhang, G. Lanty, J. S. Lauret, E. Deleporte, P. Audebert, and L. Galmiche, Acta Mater. **57**, 3301 (2009).

[13] H.-S. Kim, C.-R. Lee, J.-H. Im, K.-B. Lee, T. Moehl, A. Marchioro, S.-J. Moon, R. Humphry-Baker, J.-H. Yum, J. E. Moser, M. Grätzel, and N.-G. Park, Sci. Rep. **2**, 591 (2012).

[14] J. Burschka, N. Pellet, S.-J. Moon, R. Humphry-Baker, P. Gao, M. K. Nazeeruddin, and M. Grätzel, Nature **499**, 316 (2013).

[15] E. Edri, S. Kirmayer, D. Cahen, and G. Hodes, J. Phys. Chem. Lett. **4**, 897 (2013).

[16] M. Liu, M. B. Johnston, and H. J. Snaith, Nature (London) **501**, 395 (2013).

[17] J. H. Heo, S. H. Im, J. H. Noh, T. N. Mandal, C.-s. Lim, J. A. Chang, Y. H. Lee, H.-j. Kim, A. Sarkar, M. K. Nazeeruddin, M. Grätzel, and S. I. Seok, Nat. Photon. **7**, 486 (2013).

[18] Y.-H. Lee, X.-Q. Zhang, W. Zhang, M.-T. Chang, C.-T. Lin, K.-D. Chang, Y.-C. Yu, J. T.-W.Wang, C.-S. Chang, L.-J. Li, and T.-W. Lin, Adv. Mater. **24**, 2320 (2012).

[19] T. Ishihara, J. Takahashi, and T. Goto, Phys. Rev. B **42**, 11099 (1990).

[20] K. Tanaka, T. Takahashi, T. Kondo, K. Umeda, K. Ema, T. Umebayashi, K. Asai, K. Uchida, and N. Miura, Jpn. J. Appl. Phys. **44**, 5923 (2005).

[21] K. Tanaka, T. Takahashi, T. Kondo, T. Umebayashi, K. Asai, and K. Ema, Phys. Rev. B **71**, 045312 (2005).

[22] X. Hong, T. Ishihara, and A. Nurmikko, Solid State Commun. **84**, 657 (1992).

[23] X. Hong, T. Ishihara, and A. Nurmikko, Phys Rev. B **45**, 6961(R) (1992).

[24] K. Gauthron, J.-S. Lauret, L. Doyennette, G. Lanty, A. Al Choueiry, S. J. Zhang, A. Brehier, L. Largeau, O. Mauguin, J. Bloch, and E. Deleporte, Opt. Express **18**, 5912 (2010).

[25] Y. Wei, J. S. Lauret, L. Galmiche, P. Audebert, and E. Deleporte, Opt. Express **20**, 10399 (2012).

[26] W. Niu, A. Eiden, G. V. Parkash, and J. J. Baumberg, Appl. Phys. Lett. **104**, 171111 (2014).

[27] A. M. van der Zande, P. Y. Huang, D. A. Chenet, T. C. Berkelbach, Y. You, G.-H. Lee, T. F. Heinz, D. R. Reichman, D. A. Muller, and J. C. Hone, Nat. Mater. **12**, 554 (2013).

[28] T. Ishihara, J. Takahashi, and T. Goto, Solid State. Commun. **69**, 933 (1989).

[29] M. Hirasawa, T. Ishihara, T. Goto, K. Uchida, and N. Miura, Physica B: Condens. Matter **201**, 427 (1994).

[30] P. Blake, E. W. Hill, A. H. Castro Neto, K. S. Novoselov, D. Jiang, R. Yang, T. J. Booth, and A. K. Geim, Appl. Phys. Lett. **91**, 063124 (2007).

[31] R. R. Nair, P. Blake, A. N. Grigorenko, K. S. Novoselov, T. J. Booth, T. Stauber, R. N. M. Peres, and A. K. Geim, Science **320**, 1308 (2008).

[32] H. Li, G. Lu, Z. Yin, Q. He, H. Li, Q. Zhang, and H. Zhang, Small **8**, 682 (2012).

[33] D. B. Mitzi, Chem. Mater. **8**, 791 (1996).

[34] J. Even, L. Pedesseau, and C. Katan, ChemPhysChem **15**, 3733 (2014).

[35] G. Wei, Z. Le, Z. Yan-Ning, L. Woon-Ming, and L. Li-Min, J. Phys. Chem. C **118**, 19565 (2014).

[36] P. Umari, E. Mosconi, and F. De Angelis, Sci. Rep. **4**, 4467 (2014).

[37] J. Even, L. Pedesseau, M.-A. Dupertuis, J.-M. Jancu, and C. Katan, Phys. Rev. B **86**, 205301 (2012).

[38] See Supplemental Material at http://link.aps.org/supplemental/10.1103/PhysRevB.92.045414 for Room-temperature absorption spectra from 14 different NS samples.

[39] E. Hecht, *Optics* (Pearson Education, New York, 2012).

[40] W. T. Masselink, P. J. Pearah, J. Klem, C. K. Peng, H. Morkoç, G. D. Sanders, and Y. C. Chang, Phys. Rev. B **32**, 8027 (1985).

[41] W. Stolz, J. C. Maan, M. Altarelli, L. Tapfer, and K. Ploog, Phys. Rev. B **36**, 4301 (1987).

[42] C. Klingshirn, *Semiconductor Optics*, 3rd ed. (Springer, Berlin, 2007).

[43] L. V. Keldysh, Pis'ma Zh. Eksp. Teor. Fiz. **29**, 716 (1979) [JETP Lett. **29**, 658 (1979)].

[44] E. A. Muljarov, S. G. Tikhodeev, N. A. Gippius, and T. Ishihara, Phys. Rev. B **51**, 14370 (1995).

[45] H. Haug and S. W. Koch, *Quantum Theory of the Optical and Electronic Properties of Semiconductors*, 5th ed. (World Scientific, Singapore, 2009).

[46] J. Deslippe, M. Dipoppa, D. Prendergast, Moutinho V. O. Marcus, B. R. Capaz, and S. G. Louie, Nano Lett. **9**, 1330 (2009).

[47] F. Wu, F. Qu, and A. H. MacDonald, Phys. Rev. B **91**, 075310 (2015).

[48] P. Cudazzo, I. V. Tokatly, and A. Rubio, Phys. Rev. B **84**, 085406 (2011).

[49] H. Takagi, H. Kunugita, and K. Ema, Phys. Rev. B **87**, 125421 (2013).

[50] M. Shimizu, J.-I. Fujisawa, and J. Ishi-Hayase, Phys. Rev. B **71**, 205306 (2005).

[51] G. Berghäuser and E. Malic, Phys. Rev. B **89**, 125309 (2014).

[52] T. C. Berkelbach, M. S. Hybertsen, and D. R. Reichman, Phys. Rev. B **88**, 045318 (2013).

[53] T. Cheiwchanchamnangij and W. R. L. Lambrecht, Phys. Rev. B **85**, 205302 (2012).

[54] A. Ramasubramaniam, Phys. Rev. B **86**, 115409 (2012).

[55] H. Shi, H. Pan, Y.-W. Zhang, and B. I. Yakobson, Phys. Rev. B **87**, 155304 (2013).

[56] D. Y. Qiu, F. H. da Jornada, and S. G. Louie, Phys. Rev. Lett. **111**, 216805 (2013).

[57] K. He, N. Kumar, L. Zhao, Z. Wang, K. F. Mak, H. Zhao, and J. Shan, Phys. Rev. Lett. **113**, 026803 (2014).

[58] A. Chernikov, T. C. Berkelbach, H. M. Hill, A. Rigosi, Y. Li, O. B. Aslan, D. R. Reichman, M. S. Hybertsen, and T. F. Heinz, Phys. Rev. Lett. **113**, 076802 (2014).

[59] Z. Ye, T. Cao, K. O'Brien, H. Zhu, X. Yin, Y. Wang, S. G. Louie, and X. Zhang, Nature (London) **513**, 214 (2014).

[60] M. Ugeda, M. A. Bradley, J. Shi, S.-F. F. H. Jornada, Y. Zhang, D. Y. Qiu, W. Ruan, S.-K. Mo, Z. Hussain, Z.-X. Shen, F. Wang, S. G. Louie and M. F. Crommie [Nat. Mater. (to be published)].